Journal of Magnetism and Magnetic Materials 564 (2022) 170041

Contents lists available at ScienceDirect

Journal of Magnetism and Magnetic Materials

journal homepage: www.elsevier.com/locate/jmmm

Research article

HAMR switching dynamics and the magnetic recording quadrilemma

M. Strungaru [a,*], B.T. Nguyen [a], K. Yuanmae [b], R.F.L. Evans [a], R.W. Chantrell [a], P. Chureemart [b], J. Chureemart [b]

[a] Department of Physics, University of York, York, YO10 5DD, United Kingdom
[b] Department of Physics, Mahasarakham University, Mahasarakham, 44150, Thailand

ARTICLE INFO

Keywords:
Heat-Assisted Magnetic Recording
Heated Dot Magnetic Recording
Magnetisation switching
Bit error rate

ABSTRACT

We investigate the dynamical switching process of Heat Assisted Magnetic Recording (HAMR) by numerical calculations of switching probability using an atomistic model. Calculations show that at the elevated write temperature of HAMR there is a loss of information arising from 'backswitching': a thermodynamic phenomenon which comes into play when the ratio of the Zeeman energy to the thermal energy is insufficiently large to completely stabilise the switched direction. We consider the special case of Heated Dot Magnetic Recording, where a reduction of switching probability can be related to a bit error rate. We show that the backswitching becomes more pronounced at faster write times. Also, we show that in the case of current recording media, based on the binary alloy FePt, backswitching will be a more stringent limitation on recording density than the usually assumed thermal stability criterion.

1. Introduction

Magnetic recording, still the dominant technology for cloud storage, advances by continuous increases in recording density achieved by scaling down the grain size. This results in the famous magnetic trilemma [1], which recognises that the required increase in magnetic anisotropy, resulting from the need to ensure thermal stability of the magnetisation, must result in switching fields beyond the limits of inductive technology. The solution is Heat Assisted Magnetic Recording (HAMR) [2,3], based on highly anisotropic media heated up via a laser pulse during the writing process. The heating lowers the switching field to writeable levels, after which reduction in temperature to ambient levels restores the anisotropy and the thermal stability. Consideration of the elevated temperatures achieved in HAMR has led to an additional factor in the media design process, leading to a 'quadrilemma' [4,5]. This recognises that at elevated temperatures there is a probability of 'backswitching' when the energy difference between the states parallel and anti-parallel to the switching field is too small to ensure stability of the switched state. The fourth aspect of the quadrilemma introduces a 'thermal writability' factor: essentially a requirement that the ratio $M_s V H_{wr}/kT_{wr}$, with M_s the saturation magnetisation, V the grain volume, and H_{wr}, T_{wr} the writing field and temperature respectively, is sufficiently large to avoid backswitching.

Heated dot magnetic recording media (HDMR) is perhaps the ultimate recording medium, combining Bit Patterned Media (one single grain used per single bit) and HAMR. In the case of HDMR one can easily define a bit error rate (BER), which is given by the probability of bits that have not reached the desired orientation of the magnetisation due to thermal fluctuations. Specifically,

$$BER = 1 - P_0, \tag{1}$$

where P_0 is the switching probability. Ultimately, the maximum areal density possible to obtain via HDMR technology will be governed by the minimum BER that can possibly be achieved during reversal. Here we show that the minimum BER is given by thermal backswitching which is strongly dependent on the grain size and the write speed. We note that the BER calculated here is the 'raw' BER which is thermodynamically limited. However, in practice the actual BER is much larger due to the use of sophisticated coding schemes which determine the minimal tolerable BER: a factor beyond the scope of the current paper. In the following we will use BER to denote the *raw* bit error rate. Here we consider only the case of single grain FePt media. Suess and Schrefl [6] have extended the work of Ref. [4] to take account of more complex media, such as the exchange spring structure, finding that such designs can overcome the thermal writability at least under the assumption of thermal equilibrium magnetisation states. A further article [7] extended the calculations to bilayer structures of high T_C/ low T_C layers, again showing an improvement of achievable areal densities, using a realistic calculation of HAMR and a constant width of temperature pulse. Here we investigate a simplified experiment involving calculation of the

* Corresponding author.
E-mail address: mara.strungaru@york.ac.uk (M. Strungaru).

https://doi.org/10.1016/j.jmmm.2022.170041
Received 18 July 2022; Received in revised form 29 September 2022; Accepted 3 October 2022
Available online 7 October 2022

Table 1
Parameters used for simulating FePt.

Quantity	Symbol	Value	Units
Nearest-neighbours exchange	J_{ij}	6.71×10^{-21}	J
Anisotropy energy	k_i	2.63×10^{-22}	J
Magnetic moment	μ_S	3.23	μ_B
Thermal bath coupling	λ	0.05	
Applied field	B	1	T
Lattice spacing	a, c	2.73, 3.85	Å

switching probability and extend the calculations to small grain diameter.We restrict our calculations to an ideal case of HDMR, where all grains are identical, interactions between bits are negligible and there is no thermal destabilisation of the information between nearby bits. We also neglect magnetostatic interactions, since during the writing process at temperatures close to Tc, the magnetisation of the system is very small, hence the magnetostatic interactions are negligible compared to the applied static field. Our calculations investigate if small grain sizes (3 nm−5 nm) are physically feasible for HDMR, however the possibility to engineer technologies that, for example, deal with such small heating spot sizes goes beyond the scope of the current work.

It is important to note that in Refs. [4,5] it is assumed that the timescale of recording is sufficiently long for the magnetisation to achieve thermal equilibrium during the recording process. Here, we consider HAMR as a dynamic Field-Cooled Magnetisation (FCM) process using simulations based on an atomistic model [8] using the VAMPIRE [9] package. The dynamical switching probability and the subsequent bit error rate is explored for the FePt system, which is already the main candidate for HAMR. A possible alternative to FePt is NdFeB due to its large anisotropy. NdFeB is a permanent magnet used extensively due to its wide range of applications in the automotive and electronic industry or even in the medical sector [10], with the potential to target the global climate crisis by enabling its utilisation in electric vehicles and low carbon methods of power generation. The employment of NdFeB in HAMR applications is limited by the capacity of the mass-production of this media. Experimental investigation on how NdFeB can be produced for HAMR applications have been recently shown [11]. These studies suggest that NdFeB can be potentially used as an alternative for FePt based HAMR. NdFeB is also a good candidate to tackle the magnetic quadrilemma, since the BER is affected by the saturation magnetisation, which is larger for NdFeB than FePt. We show that the switching probability and consequent BER is strongly dependent on the cooling rate. This is illustrated using a simple semi-analytic model. Switching probability is shown to be determined by the time during the cooling process between the Curie temperature T_C and the magnetic blocking temperature, which is of the order of tens of picoseconds at maximum.

2. Computational model

The general formulation of atomistic spin models [8] employs a lattice of fixed length atomic spins on a regular lattice, interacting via a spin Hamiltonian of the form:

$$\mathcal{H} = \sum_{i<j} J_{ij}\hat{\mathbf{m}}_i \cdot \hat{\mathbf{m}}_j + \sum_i k_i \hat{\mathbf{e}} \cdot \hat{\mathbf{m}}_i - \mu_s \sum_i \mathbf{H} \cdot \hat{\mathbf{m}}_i, \tag{2}$$

where $\hat{\mathbf{m}}_i, \hat{\mathbf{m}}_j$ are unit vectors describing the direction of local moments i, j, J_{ij} is the Heisenberg exchange interaction between neighbouring spins, μ_s is the atomic spin moment and $\mathbf{H}$ is the externally applied magnetic (induction) field. The second term represents the (uniaxial) anisotropy contribution with an easy direction $\hat{\mathbf{e}}$ and magnitude k_i.

The dynamics of each individual spin is obtained by integrating the Landau–Lifshitz–Gilbert (LLG) equation of motion:

$$\frac{\partial \hat{\mathbf{m}}_i}{\partial t} = -\frac{\gamma}{1+\lambda^2}\left[\hat{\mathbf{m}}_i \times \mathbf{H}_{\mathbf{eff}} + \lambda \hat{\mathbf{m}}_i \times (\hat{\mathbf{m}}_i \times \mathbf{H}_{\mathbf{eff}})\right], \tag{3}$$

where λ controls the damping and represents the coupling of spins to a heat bath through which energy can be transferred into and out of the spin system. $\mathbf{H}_{\mathbf{eff}}$ is the effective field acting on each spin obtained by differentiating the Hamiltonian (Eq. (2)) with respect to the atomic spin moment and accounts for the interactions within the system. Finite temperature effects are included under the assumption that the thermal fluctuations are non-correlated and hence can be described by a white noise term. This is expressed as a Gaussian distribution in 3 dimensions whose first and second statistical moments of the distribution are:

$$\langle \xi_{ia}(t) \rangle = 0, \tag{4}$$

$$\left\langle \xi_{ia}(t)\xi_{jb}(t') \right\rangle = \frac{2\lambda k_B T}{\mu\gamma}\delta_{ij}\delta_{ab}\delta(t-t'), \tag{5}$$

where i, j label spins on the respective sites, $a, b = x, y, z$ are the vector component of $\vec{\xi}$ in Cartesian coordinates, t, t' are the time at which the Gaussian fluctuations are evaluated, T is the temperature, δ_{ij} and δ_{ab} are Kronecker delta and $\delta(t-t')$ is the delta function. Eq. (4) represents the average of the random field, whilst Eq. (5) gives the variance of the field, which is a measure of the strength of its fluctuations. The thermal contribution is added to $\mathbf{H}_{\mathbf{eff}}$ at each timestep.

3. Results

3.1. Heated dot recording media: FePt and NdFeB

To model the heated dot experiments we apply a temperature pulse that is Gaussian in time and a negative out-of-plane magnetic field of $B = -1$ T (Fig. 1, left panel, right axis). The temporal variation of the temperature pulse is a Gaussian of width $\sigma = t_p$, centred around 3σ $(3t_p)$ and is defined as $T(t) = T_{min} + (T_{max} - T_{min})\exp\left(-(\frac{t-3t_p}{t_p})^2\right)$, where t represents the time, t_p represents the pulse width and $T_{min,max}$ the minimum and maximum temperature of the pulse. Under the effect of thermal fluctuations, the system will be demagnetised (Fig. 1, left panel, left axis), hence the anisotropy field of the system will decrease. This will allow the magnetisation to reverse in a smaller magnetic field, such as $B = -1$ T. By repeating the experiment for an ensemble of 50 identical grains with different thermal field random seeds, we observe that there are grains for which the magnetisation is not switched, even in a negative field of 1 T (Fig. 1, right panel). This is the physical manifestation of the backswitching phenomenon. The grains that have not switched lead to a non-zero bit error rate.

The switching mechanism at high temperatures can be understood by analysing the energy barrier schematics in Fig. 2. In the absence of an applied field, for an uniaxial anisotropy there are two equal energy minima, as shown in Fig. 2, left panel. In this case, under the influence of large thermal excitation, the magnetisation can be in either positive or negative orientation, as the thermal energy is sufficient for the system to cross from one energy minimum to another. Under the application of a negative field, Fig. 2, right panel, the energy barrier from the positive to the negative magnetisation is lowered hence the system's magnetisation can cross to the negative magnetisation energy minimum. This minimum corresponding to the negative magnetisation has the lowest energy, hence the system's magnetisation will prefer to stay in this orientation. However for high temperature pulses, the thermal energy can be sufficiently high for the system to make a crossing of the energy barrier back to the positive magnetisation energy minimum, even if the energy difference from the negative to the positive orientation is larger than in the opposite direction. If the system is then cooled sufficiently fast (as in the case corresponding to narrow temperature pulse widths) the system will remain blocked in the energy minimum corresponding to the positive orientation of the magnetisation, anti-parallel to the direction of the applied field; this can lead to a non-zero bit error rate.

We next calculate via atomistic simulations of HDMR the switching probability (defined as the ratio between how many grains have

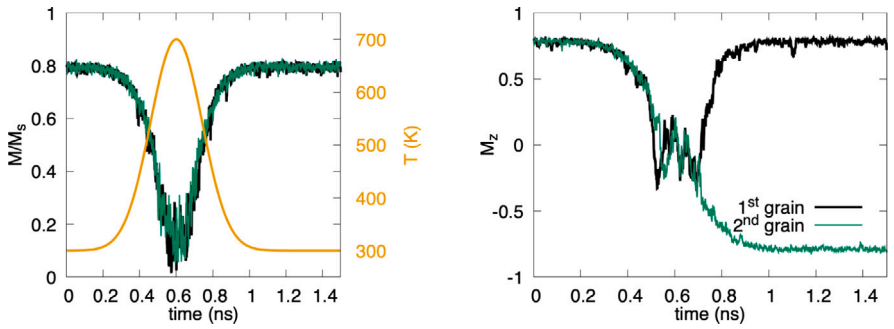

Fig. 1. Example of heated dot magnetic simulations for a temperature pulse width of 200 ps and a maximum temperature of T_{max} = 700 K in an out-of-plane magnetic field of $B = -1$ T for two FePt cylindrical grain of 3 nm × 3 nm × 5 nm; The left panel shows the temperature profile during the simulation (orange—right axis) and the total magnetisation (green/black—left axis). The right panel shows the z component of the magnetisation. For the same simulation conditions, with a different sequence of pseudo-random numbers, either a switched or not-switched state can be obtained—right panel.

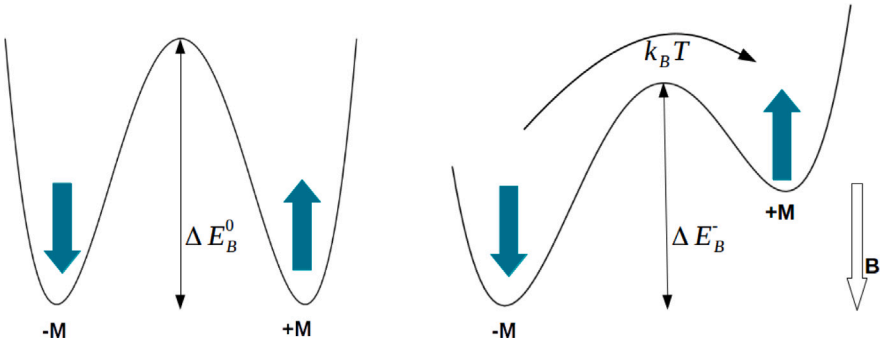

Fig. 2. Schematics of energy barrier without an applied field (left panel) and with an applied field (right panel).

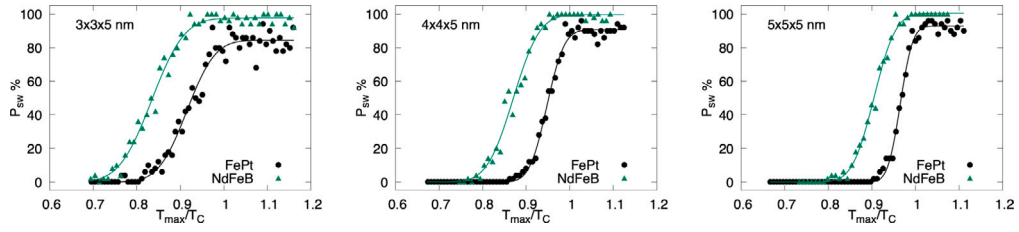

Fig. 3. Switching probability calculations for FePt (black points) and NdFeB (green points) for 50 cylindrical grains of 5 nm height. The switching probability is calculated for varying maximum temperature of the heat pulse T_{max} normalised by the Curie temperature T_C of individual materials and system size. The temperature pulse width is 200 ps.

reversed against the total number of grains) for different temperature pulses. By varying the maximum temperature of the pulse (T_{max}) we can obtain the switching probability curves for specific pulse widths. The systems we model are represented by cylindrical grains of 5 nm height and varying diameter (3 nm to 5 nm). The model used for FePt is based on that developed by Mryasov et al. [12] and used in previous work [13], the model parameters being presented in Table 1. The FePt Hamiltonian includes just nearest neighbour exchange interaction which gives a Curie temperature of about 720 K for a bulk system. The atomistic model of NdFeB using parameters given in Ref. [14], where the temperature dependence of the magnetic properties has been investigated. Further details of the model are given in Ref. [15,16]. The magnetic Hamiltonian used for NdFeB contains exchange interactions between the Fe–Fe and Fe–Nd sites, the B atoms being considered non-magnetic and the interaction between Nd sites being negligible. The very large anisotropy of NdFeB (≈17 T) comes mainly from the Nd sites [17] and considers second and fourth order uniaxial anisotropy contributions, the Fe sites contributing only weakly to the overall anisotropy. The Curie temperature is lower in the case of NdFeB at ≈585 K.

Fig. 3 shows the switching probability for both FePt and NdFeB HDMR, calculated for 50 non-interacting grains with a temperature pulse width of 200 ps. The dimensions of the grain varies from 3 nm to 5 nm in diameter. The height of the grain is kept constant at 5 nm size. Since NdFeB and FePt have different Curie temperatures, to be able to compare the switching probabilities of the two materials, the maximum temperature of the pulse has been normalised by the Curie temperature T_C of individual materials and system size, shown in Table 2. The Curie temperature has been extracted from the equilibrium susceptibility calculated numerically via Monte-Carlo simulations with a temperature resolution of 10 K. The susceptibility has been interpolated via a quadratic function, that takes into account in total 9 points for the interpolation. We observe in Fig. 3 that in the case of FePt, the switching probability is always lower than 100% and its saturation value decreases with decreasing diameters. However, NdFeB has an increased switching probability even for small system sizes, suggesting that it could be more suitable for HDMR. By investigating how we can improve the switching probability in FePt in Section 3.2, we show that increased saturation magnetisation helps to overcome the thermal writeability problem of the quadrilemma. Hence, we can conclude that in the case of NdFeB, the decreased BER is a consequence of the larger saturation magnetisation.

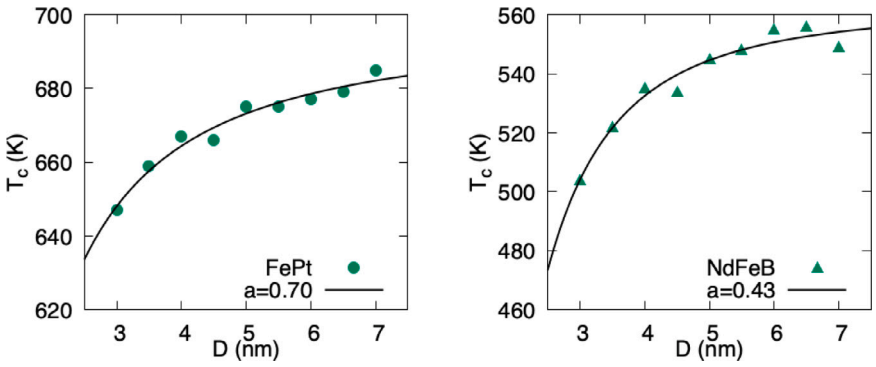

Fig. 4. Curie temperature as a function of grain diameter for FePt (left panel) and NdFeB (right panel). The black line shows the fit to the finite size scaling law $T_c(D) = T_c^{\infty}\left[1-(d_0/D)^{1/a}\right]$ from Ref. [18]. The fitting parameters are $T_c^{\infty} = 696.5$ K, $d_0 = 0.46$ nm, $a = 0.7$ for FePt and $T_C^{\infty} = 562.2$ K, $d_0 = 1.13$ nm, $a = 0.43$ for NdFeB.

Table 2
The Curie temperature of FePt and NdFeB for different grain diameters.

D (nm)	T_C (K), FePt	T_C (K), NdFeB
3	647	504
4	667	535
5	675	545

Fig. 4 shows the variation of the Curie temperature as a function of the grain diameter D extracted from the interpolation of the equilibrium magnetic susceptibility. The curves have been fitted to the finite size scaling law $T_c(D) = T_c^{\infty}\left[1-(d_0/D)^{1/a}\right]$ from Ref. [18], where Tc^{∞} represents the Curie temperature that would be obtained for $D \to \infty$ (in this case a thin film system of thickness 5 nm), d_0 is related to the unit cell size and a represents the critical scaling exponent. For FePt, the scaling exponent $a = 0.7$ obtained from the fit is comparable to Ref. [18] ($a = 0.79$), slightly lower in value presumably due to the 5 nm thickness of the systems modelled here. Interestingly, we observe that in the case of FePt the exponent a is larger than in the case of NdFeB, suggesting stronger finite size effects in both the magnetisation and the BER. Note that for the switching probability calculations, when normalising the pulse temperature to Tc, we use the numerical values calculated for the specific system sizes, rather than the fitted curve.

To systematically analyse the BER, we can fit the switching probability plots to a cumulative distribution function (CDF) defined as:

$$f(x) = \frac{P_0}{2}\left(1 + \mathrm{erf}\left(\frac{x-\bar{x}}{\sigma\sqrt{2}}\right)\right) \tag{6}$$

$$\mathrm{erf}(x) = \frac{2}{\pi}\int_0^z \exp(-t^2)dt, \tag{7}$$

where P_0 is the maximum switching probability, σ defines the width of the transition and $\bar{x}$ the mean transition temperature. In the ideal case, the maximum switching probability parameter should be $P_0 = 1$ (100%) and the transition should be abrupt, hence $\sigma = 0$ K. In reality, thermal and finite size effects lead to a relatively wide transition 15 K–30 K and switching probability less than unity. An example of fitting the switching probability calculations via the cumulative distribution function is shown in Fig. 5 (left panel). After the fit, the BER can be then calculated from the switching probability via Eq. (1), where P_0 is obtained by fitting to Eq. (6).

Fig. 5 (right panel) shows the BER as function of the system diameter for both FePt and NdFeB. The BER for NdFeB is considerably smaller than in the case of FePt suggesting that NdFeB could be more successfully used in HDMR. Since NdFeB has higher saturation magnetisation and lower Curie temperature than FePt, we can expect that these magnetic properties might influence the switching.

3.2. Improved switching probability in FePt

Evans et al. [4] have suggested that the BER can be expressed in terms of the equilibrium magnetisation m_e as $BER = 0.5(1 - m_e)$. Via the Master equation, the BER for a system with perfectly aligned easy axis is given by:

$$BER = \exp\left(-2\frac{M_S V \mu_0 H_{wr}}{k_B T_{wr}}\right) \tag{8}$$

Eq. (8) is derived in thermal equilibrium, which is not the case of HDMR calculations, since HAMR is an intrinsically dynamical process. However in the first instance, Eq. (8) can be used as an approximation to understand which magnetic parameters control the BER. We observe that a decreased BER can be obtained by either increasing the writing field H_{wr} or the magnetisation of the system $\mu = M_S V$. We distinguish that an increase in the volume of the system leads to smaller BER, this being confirmed by the numerical results in Fig. 5, right panel that describes the dependence of BER on the diameter. Ultrahigh areal densities require a reduction in grain diameter, hence a possibility to increase the volume is by an increased height of the grains, this being limited by the necessity of coherent reversal of the grains. Thus in reality, there is not much space to alter the volume, hence we next investigate the effect of the magnetic parameters that are intrinsically different between FePt and NdFeB, such as M_s, T_C (which is related to the thermal fluctuations $k_B T$ in Eq. (8)) and damping, and the pulse properties, such as the pulse duration and applied field, being able to cover, in this way, all possible effects in Eq. (8). The results are summarised in Fig. 6 and unless otherwise stated, the simulations are for a pulse width $t_p = 200$ ps and the parametrisation shown in Table 1.

NdFeB showed a considerably improved BER, its saturation magnetisation being higher than in the case of FePt, hence we start with the effect of M_S on the BER. The saturation magnetisation of FePt has been varied by artificially changing the magnetic moment of Fe atoms in the material. The magnetic moment used for FePt is $\mu = 3.23\mu_B$ which gives a saturation magnetisation of $M_S = 10.43 \times 10^5$ A/m = 1043 emu/cm^3. The saturation magnetisation is calculated as the magnetic moment per unit cell divided by the volume of the unit cell. We have calculated the switching probabilities and the BER for 2 more values of the saturation magnetisation corresponding to $M_S = 5.21 \times 10^5$ A/m (for $\mu = 1.61\mu_B$) and $M_S = 20.86 \times 10^5$ A/m (for $\mu = 6.46\mu_B$). Fig. 6,(a) shows that with increasing magnetic moment there is an increase in the maximum switching probabilities, which leads to decreased values of BER - Fig. 6,(b), hence one alternative for improving the performance of HDMR is to find materials with increased M_S. This proves that the improved performance of NdFeB comes from the increased saturation magnetisation.

Another difference between NdFeB and FePt is given by the Curie temperature (585 K for NdFeB compared to 720 K for FePt for bulk systems). A decreased Curie temperature for the FePt was obtained

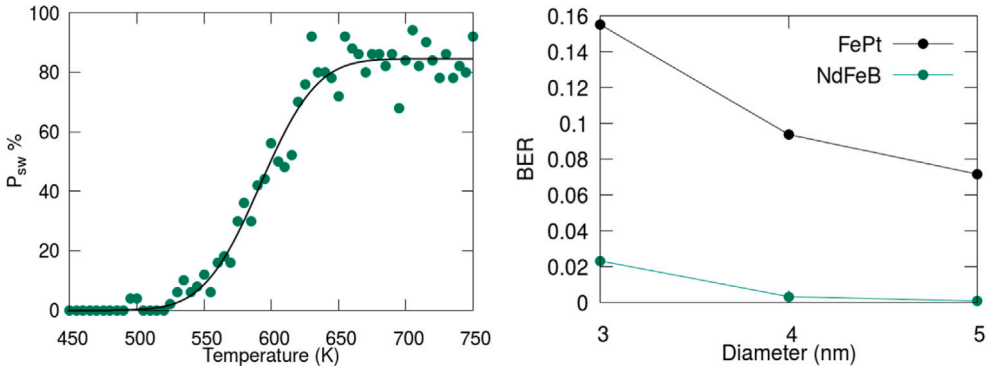

Fig. 5. BER calculation for FePt and NdFeB; (left panel) Example of fitting of the switching probability of FePt grains of dimension 3 nm × 3 nm × 5 nm via the cumulative distribution function in Eq. (6). (right panel) The variation of the bit error rate calculated via Eq. (1) as function of the system size for FePt and NdFeB systems.

by scaling the exchange interaction to a value that will correspond to the Curie temperature of NdFeB (since the Curie temperature varies linearly with the nearest-neighbour exchange interaction [8,19]). The decreased Curie temperature in FePt leads to a small decrease in the values of BER - Fig. 6,(d), but not sufficiently to favour the 3 nm grains for their usage in HDMR; this suggests that M_S is more important. By choosing increased damping and pulse width values, the system can evolve more quickly to thermal equilibrium, which consequently will lead to a decreased BER, as shown in Fig. 6,(e,f) (the effect of damping) and Fig. 6,(g,h) (the effect of the pulse width). With increasing damping, the probability of the particle to remain blocked in a positive magnetisation minimum due to the fast cooling of the system is reduced, the same happening with increased pulse widths, since the system can more easily follow the temporal evolution of the temperature pulse, reducing significantly the BER. This effect has also been shown in Ref. [20] where the influence of the Gilbert damping on the signal-to-noise ratio has been analysed for HAMR.

With increasing applied field the BER is further reduced - Fig. 6,(i,j), as suggested by Eq. (8), however such large values of applied magnetic field are not yet accessible because no practical material has been found with a saturation magnetisation larger than the limit of the Slater–Pauling curve. The development of all-optical-switching technologies [21] and the subsequent high internal magnetic fields developed during the process either by non-polarised or circularly polarised light (as in the Inverse Faraday Effect) might lead to materials that exhibit low required BER due to the development of large internal fields. The systematic investigation performed above suggests that in order to obtain ultrahigh areal densities via HDMR technologies for small grain sizes it is crucial to accurately control the BER of the system via an increased saturation magnetisation and damping, in addition to the high anisotropy which is necessary for the thermal stability of the grains. Increasing the pulse width leads to a decreased BER, however, from the technological point of view, also leads to a much lower writing speed. The interplay between all these parameters that control the BER needs to be taken into account while exploring the limits of areal densities of the recording media technologies. By considering numerical calculations of BER as presented in this section, we next reassess the maximum areal density that can be obtained in HDMR.

3.3. Maximum areal densities for HDMR

The analytical areal density calculations (AD) in Ref. [4] are given by:

$$AD = V^{-2/3}\epsilon \tag{9}$$

where $\epsilon = 0.5$ is the areal packing fraction, V is the volume which has been expressed based on the area of a cubic grain. The volume can be extracted from Eq. (8) $V = \ln[(BER)^{-1}]k_B T_{wr}/(M_S(T)\mu_0 H_{wr})$ and used in Eq. (9) leading to the following expression:

$$AD = \left(\frac{2M_S(T)\mu_0 H_{wr}}{k_B T_{wr}\ln[(BER)^{-1}]}\right)^{2/3}\epsilon. \tag{10}$$

In Eq. (10), the writing temperature T is considered as being 10 K lower than the Curie temperature of the system, which is a rough approximation and can lead to higher areal densities. A better description is given by the usage of the blocking temperature T_B, which is the temperature at which the transition towards the superparamagnetic state happens. An initial estimation of the blocking temperature can be deduced from the Arrhenius–Néel relaxation equation, where $T_B = KV/(k_B \ln(\tau f_0))$, τ being the relaxation time in a constant temperature and f_0 the attempt frequency ($f_0 = 10^9 - 10^{12}$ s^{-1}). For systems where the temperature is not constant, such as in HAMR, the following rate dependent estimation of the blocking temperature needs to be used, as suggested by Chantrell and Wohlfarth [22]:

$$\frac{KV}{k_B T_B}(1 - H/H_K)^2 = \ln\left[\frac{f_0 \dot{T}^{-1}(KV/k_B)}{(\frac{KV}{k_B T_B})^2(1 - H/H_K)^2}\right]. \tag{11}$$

In Eq. (11), $\dot{T}^{-1}$ is the rate of temperature variation which we approximate as constant. We can calculate numerically the blocking temperature from Eq. (11) using the temperature variation of the anisotropy as $K(T) \sim m(T)^3$ for uniaxial anisotropy of FePt in the absence of two-ion anisotropy. The temperature dependence of the magnetisation is considered $m(T) = \left(1 - \frac{T}{T_C(D)}\right)^{\beta}$, $\beta = 0.33$ and a Curie temperature of $T_C(3\text{ nm}) = 647$ K for a 3 nm size grain. Additionally, we consider an attempt frequency of $f_0 = 10^{12}$ s^{-1} and a linear cooling of the system from 750 K to 300 K in 0.3 ns in a field of $H = 1$ T, since in Eq. (11) it enters a constant rate $\dot{T}^{-1}$. The solution of Eq. (11) will be given by the intersection between the temporal variation of the blocking temperature calculated in Eq. (12) with the temporal evolution of the temperature:

$$T_B = \frac{KV(1 - H/H_K)^2}{k_B \ln\left[\frac{f_0 \dot{T}^{-1}(KV/k_B)}{(\frac{KV}{k_B T(t)})^2(1 - H/H_K)^2}\right]}, \tag{12}$$

where the anisotropy constant and anisotropy field depend on the temperature that has a temporal evolution - $T(t)$, which is approximated with a linear function. Numerically, the blocking temperature of the FePt granular system of 3 nm diameter is found to be $T_B = 548$ K. For diameters of 4 nm and 5 nm, blocking temperatures of $T_B = 594$ K and $T_B = 619$ K were extracted. The areal densities corresponding to the grain sizes investigated here are: AD(3 nm) = 45.6 Tb/in^2, AD(4 nm) = 25.6 Tb/in^2, AD(5 nm) = 16.4 Tb/in^2.

We note that, statistically, there will be a distribution of blocking temperature T_B which arises from the random switching path through the phase space. The value of blocking temperature in Eq. (12) represents the mean value. Returning now to the areal density calculations,

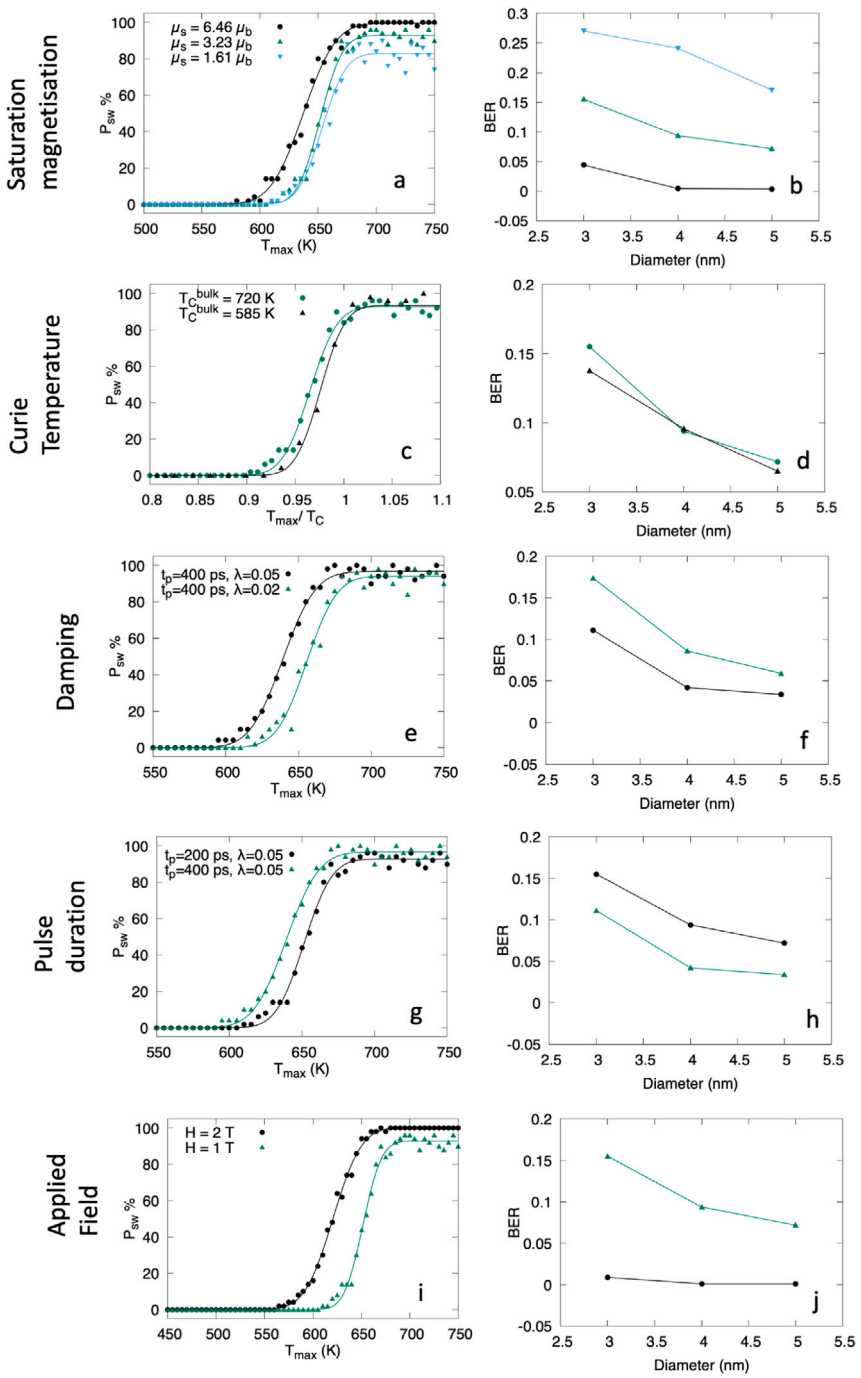

Fig. 6. The effect of different magnetic properties on the switching probability in FePt (left column—for grain size 5 nm × 5 nm × 5 nm) and BER as function of system size (right column).

using the blocking temperature calculated above, we can compare the analytical variation of the areal density as function of BER given by Eq. (10) to the BER values calculated numerically for different grain diameters. Fig. 7 shows that the BER obtained via numerical calculations corresponds to AD about 50% lower than in the case of the analytical calculations, for temperature pulse widths of t_p = 200 ps. Doubling the pulse width to t_p = 400 ps, the numerical BER is closer to the analytical values. This is due to the fact that, in the analytical calculations thermal equilibrium is assumed, which is not the case in practice. The dynamic behaviour of the magnetic properties will strongly influence the maximum areal density that can be achieved. Nevertheless, it is possible to further develop this proposed model by including distribution effects (of saturation magnetisation, anisotropy, T_C etc.) using macro-spin models based on the Landau–Lifshitz–Bloch equation, as in Ref. [23] - this type of numerical simulation will offer a good perspective of the important parameters that control the blocking temperature, BER and the ultimate limit for recording media.

4. Conclusion

We have presented a model of the dynamics of the HAMR process, with particular emphasis on heated dot magnetic recording, which allows estimation of the raw BER from the switching probability. The results demonstrate the importance of the 'thermal writability' arising from thermal backswitching of the magnetisation, leading to write errors. Previous work [4,5] was based on the simplifying assumption of

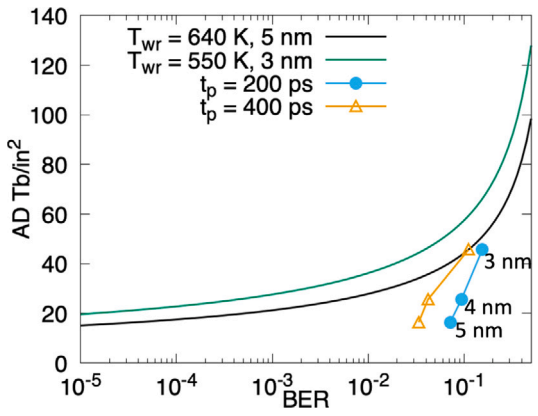

Fig. 7. Analytical and numerical areal density calculations for HDMR; The writing temperature is given by the blocking temperature calculated via Eq. (12) for two diameters of the grains (3 and 5 nm). Smaller areal densities are obtained numerically for the same values of BER, due to the dynamic variation of the temperature and magnetic properties.

the magnetisation achieving the thermal equilibrium value at the estimated blocking temperature. A simple modification of the semi-analytic model by treating HAMR as a field-cooled magnetisation process has also been developed. For long pulse widths this gives slightly higher predicted values of areal density than in Ref. [4] due to the lower predicted blocking temperature.

We find that the HAMR behaviour follows the analytical approach in terms of the dependence on material parameters. In particular the factor $M_s V H_{wr}/k_B T_{wr}$, which governs the thermal writability, is a dominant factor, reflected in the fact that NdFeB gives improved results over FePt. However, our calculations show the importance of the dynamics in the sense that, as shown in Fig. 7, the BER increases rapidly with shorter temperature pulse widths. In principle, 3 nm × 3 nm × 3 nm grains could be used for high density recording, but this would require tolerance of a (raw) BER of 10^{-1}, which would seem technically challenging. It seems likely that, although such grains would be marginally viable in terms of thermal stability, they are likely to be ruled out by their thermal writability, which becomes the more important factor. Improving this factor might be done via design, such as the high T_C/ low T_C design investigated by Suess et al. [7]. However, even here the dynamical behaviour of the design needs to be carefully investigated. In Ref. [7], it was observed that the high T_C layer (Fe) required a very high damping to achieve a reliable switching, as also found by Ababei et al. [24]. Essentially this is because the thermal writability is provided by the Fe layer, which must precess into the field direction: a limiting factor if many precession cycles are required to switch direction, especially given that switching must occur on the timescale of at most a few hundred ps. Single grains can switch using the linear reversal mechanism [25,26] which is much faster than precessional reversal, giving single grain media an intrinsic advantage. This must be considered an important factor in materials design. The region between T_C and the blocking temperature, traversed in tens or a hundred ps, depending on the rate of temperature reduction, is clearly an important area for investigation.

CRediT authorship contribution statement

M. Strungaru: Conceptualisation, Methodology, Software, Investigation, Writing – original draft, Writing – review & editing. **B.T. Nguyen:** Software, Investigation, Writing – review & editing. **K. Yanmae:** Software, Investigation, Writing – review & editing. **R.F.L. Evans:** Conceptualisation, Methodology, Software, Supervision, Project administration, Funding acquisition, Writing – review & editing. **R.W. Chantrell:** Conceptualisation, Methodology, Writing – original draft, Supervision, Project administration, Funding acquisition, Writing – review & editing. **P. Chureemart:** Conceptualisation, Methodology, Supervision, Project administration, Funding acquisition, Writing – review & editing. **J. Chureemart:** Methodology, Supervision, Project administration, Funding acquisition, Writing – review & editing.

Declaration of competing interest

The authors declare that they have no known competing financial interests or personal relationships that could have appeared to influence the work reported in this paper.

Data availability

Data will be made available on request.

Acknowledgements

The authors gratefully acknowledge the funding from Seagate Technology (USA) and from Transforming Systems, United Kingdom through Partnership Programme of the Royal Academy of Engineering under Grant No. TSP1285 and Seagate Technology (Thailand). Financial support of the Advanced Storage Research Consortium (USA) is gratefully acknowledged.

Numerous simulations for this work were undertaken on the Viking Cluster, which is a high performance compute facility provided by the University of York. We are grateful for computational support from the University of York High Performance Computing service, United Kingdom, Viking and the Research Computing team, United Kingdom.

References

[1] H. Richter, J. Phys. D: Appl. Phys. 40 (9) (2007) R149.
[2] R. Rottmayer, S. Batra, D. Buechel, W. Challener, J. Hohlfeld, Y. Kubota, L. Li, B. Lu, C. Mihalcea, K. Mountfield, K. Pelhos, C. Peng, T. Rausch, M. Seigler, D. Weller, X.-M. Yang, IEEE Trans. Magn. 42 (10) (2006) 2417–2421.
[3] G. Ju, Y. Peng, E.K.C. Chang, Y. Ding, A.Q. Wu, X. Zhu, Y. Kubota, T.J. Klemmer, H. Amini, L. Gao, Z. Fan, T. Rausch, P. Subedi, M. Ma, S. Kalarickal, C.J. Rea, D.V. Dimitrov, P.-W. Huang, K. Wang, X. Chen, C. Peng, W. Chen, J.W. Dykes, M.A. Seigler, E.C. Gage, R. Chantrell, J.-U. Thiele, IEEE Trans. Magn. 51 (11) (2015) 1–9.
[4] R. Evans, R.W. Chantrell, U. Nowak, A. Lyberatos, H.-J. Richter, Appl. Phys. Lett. 100 (10) (2012) 102402.
[5] H. Richter, A. Lyberatos, U. Nowak, R.F.L. Evans, R.W. Chantrell, J. Appl. Phys. 111 (3) (2012) 033909.
[6] D. Suess, T. Schrefl, Appl. Phys. Lett. 102 (16) (2013) 162405.
[7] D. Suess, C. Vogler, C. Abert, F. Bruckner, R. Windl, L. Breth, J. Fidler, J. Appl. Phys. 117 (16) (2015) 163913.
[8] R.F. Evans, W.J. Fan, P. Chureemart, T.A. Ostler, M.O. Ellis, R.W. Chantrell, J. Phys.: Condens. Matter 26 (10) (2014) 103202.
[9] 2020. VAMPIRE Software Package V5 https://vampire.york.ac.uk.
[10] D. Brown, B.-M. Ma, Z. Chen, J. Magn. Magn. Mater. 248 (3) (2002) 432–440.
[11] T. Tsuchida, J. Fukushima, S. Hinata, Y. Hayashi, S. Saito, H. Takizawa, J. Appl. Phys. 127 (10) (2020) 103901.
[12] O. Mryasov, U. Nowak, K. Guslienko, R. Chantrell, Europhys. Lett. 69 (5) (2005) 805–811.
[13] M. Strungaru, S. Ruta, R.F. Evans, R.W. Chantrell, Phys. Rev. Appl. 14 (2020) 014077.
[14] Q. Gong, M. Yi, R.F.L. Evans, B.-X. Xu, O. Gutfleisch, Phys. Rev. B 99 (2019) 214409.
[15] S. Westmoreland, Atomistic Calculations of Magnetic Properties of Rare-Earth Transition-Metal Permanent Magnets (Ph.D. thesis), University of York, 2018.
[16] S. Westmoreland, R. Evans, G. Hrkac, T. Schrefl, G. Zimanyi, M. Winklhofer, N. Sakuma, M. Yano, A. Kato, T. Shoji, et al., Scr. Mater. 148 (2018) 56–62.
[17] D. Haskel, J. Lang, Z. Islam, A. Cady, G. Srajer, M. Van Veenendaal, P. Canfield, Phys. Rev. Lett. 95 (21) (2005) 217207.
[18] O. Hovorka, S. Devos, Q. Coopman, W. Fan, C. Aas, R. Evans, X. Chen, G. Ju, R. Chantrell, Appl. Phys. Lett. 101 (5) (2012) 052406.
[19] D. Garanin, Phys. Rev. B 53 (17) (1996) 11593.
[20] O. Muthsam, F. Slanovc, C. Vogler, D. Suess, J. Magn. Magn. Mater. (2020) 167125.
[21] T. Ostler, J. Barker, R. Evans, R. Chantrell, U. Atxitia, O. Chubykalo-Fesenko, S. El Moussaoui, L. Le Guyader, E. Mengotti, L. Heyderman, et al., Nature Commun. 3 (1) (2012) 1–6.
[22] R. Chantrell, E. Wohlfarth, Phys. Status Solidi (A) 91 (2) (1985) 619–626.

[23] S. Rannala, A. Meo, S. Ruta, W. Pantasri, R. Chantrell, P. Chureemart, J. Chureemart, Comput. Phys. Comm. 279 (2022) 108462.
[24] R.-V. Ababei, M.O.A. Ellis, R.F.L. Evans, R.W. Chantrell, Phys. Rev. B 99 (2019) 024427.
[25] N. Kazantseva, D. Hinzke, R.W. Chantrell, U. Nowak, Europhys. Lett. 86 (2) (2009) 27006.
[26] M.O.A. Ellis, R.W. Chantrell, Appl. Phys. Lett. 106 (16) (2015) 162407.